Reaction of uranium with poly-hydroxy-aromatic groups on particles through mono- and multi- dentate surface complexes on the basis of pH and redox potential: a modelling approach.

Steven McGowan[1], Claude Degueldre[1*], Farid Aiouache[1]
[1]Engineering Department, Lancaster University, Lancaster, LA1 4YW, UK

*Corresponding authors: c.degueldre@lancaster.ac.uk

Abstract

The analytical approach that was proposed in our recent paper has been applied to simulate effects of pH and redox potential (E) on the sorption of uranium onto potentially redox active bioorganic model particles in saline or other aquatic environments. Specifically herein, it is applied to the mono- and poly-hydroxy-aromatic (polyphenolic) sites which account for approximately 30% of bioorganic site capacity. The derived expression is aimed to avoid use of the classical approach of sorption, which requires experimental data and empirical models. The expression provides a distribution coefficient (K_d e.g. mL g^{-1}) as function of pH, E and soluble ligand concentration by considering a surface complexation model on mono- or multi-dentate complexation surface sites $>Su(OH)_c$. The application of the model uses correlations between the surface complexation constants and hydrolysis constants, for all potential species and all form of sorption sites. The model was used to quantify the uranium sorption onto hydroxy-benzene, dihydroxy-benzene, and dihydroxy-naphthalene sites with or without carbonates in solution. The latter is the primary interfering reagent in waters that decreases Log K_d. The calculated distribution coefficients were found sensitive to both pH and E and very sensitive to the presence of carbonates. The reduction of uranium U(VI), and its carbonate complexes, to U(IV) during sorption was simulated by decreasing the redox potential. It was found that the transition phase between U(VI) and U(IV) was generally below the redox stability limits of water. However, the reduction of U(VI) to U(IV) was found to be potentially associated with their reaction with the polyphenols, decreasing the redox potential subsequently. The calculated sorption coefficient values were validated using the values reported in literature for the sorption of uranium onto specific adsorbents. The methodology of the simulation is also applicable to the sorption of other redox sensitive elements, and with the addition of a scaling factor, it would allow the predictions of co-complexation phenomena by employing relevant site formulations. The oxidation of mono-hydroxy- benzene in di-hydroxy-benzene enhances the sorption of uranium by a factor 10^6 which may be applied to its extraction from seawater. XX

Keywords: uranium sorption coefficient; redox potential; surface complexation; metal sorption on biomass; multi-dentate surface complex; poly-hydroxy-aromatic;

1 Introduction

Natural organic matter controls metal speciation and toxicity in various bioorganic systems. The bioorganic molecules that make up natural materials have large and complex structures but are produced through an iterative mechanism using simple basic units, allowing use of simple analogues to simulate the general structure by mapping representative units of the binding site. By bulk capacity, the most common binding site in plant biomass is the carboxylic acids, as illustrated by Pontoni et al. (2022), and the closest next common acid site is the polyphenolic structure. The structure of the carboxylic acids were found to serve as barrier to harmful elements and to offer consistent binding capacity over the pH range that the biomaterial meet, as reported by McGowan et al. (2022). Alternatively, free

polyphenolic compounds in biomaterials are more reactive due to their labile structures and act as aromatic component, compensating the lower density within the materials.

In addition to the direct surface complexation, many chemical structures in biomass are acting as reducing agents intended to control the redox potential such as the conversion of the mobile forms of uranium to immobile ones, helping acceleration of the deposition and minimizing release, and thus significantly increasing the effectiveness of the materials beyond the bulk capacity, see Lovley et al. (1991) and Senko et al. (2002). Furthermore, the biomaterials often include nutritional benefits for the microorganisms, which boost also the deposition processes as reported by Senko et al. (2002).
Polyphenolics in the natural resources are attributed to four classes of hydroxy groups on aromatic rings, including phenolic acids, such as flavonoids Ververidis et al. (2007), stilbenes, such as diethylstilbestrol and dienestrol, see Bjorkman and Taylor (2018), and lignans, as per Saleem et al. (2005). In the context of uranyl sorption on colloidal materials, surface complexation, reductive and colloid aggregation/precipitation have been reported by Mathew et al. (2016) owing to the strong affinity for extraction and high complexation potential, driven by their antioxidant properties (which helps reduce the valence state of the adsorbed metal ion) and peptization/flocculation effect (Sakagushi and Nakajima, 1987). For example, Quercetin [$(H_2C_6(OH)_2)O(COHCOHC)(H_3C_6(OH)_2)$], a polyphenol present in a wide range of materials, such as citrus fruits, wine tannin, or bark tannins, binds to the ions, complexes and thus bridges two or more molecules, resulting in permanent binding and enhancement of the extraction. The family of tannin-loaded biomaterials through the berries, barks, malt, and tealeaf biomasses have been demonstrated to load uranium at approximately 100-300 mg per kg, as per McGowan et al. (2022).

In order to simplify estimation of mass balance in the modelling, the partition coefficient, K_d, is commonly used, and much of literature on K_d of radionuclides was relevant to remediation applications and inherently used conservative approaches by empirical models of sorption, as per McKinley and Scholtis (1993). However, for accurate modelling, a generalised model is necessary. As *Kd* is an emergent property that is based on molecular mechanistic approach, it is possible, using certain core factors, to correlate K_d to other measured properties and model sorption of uranium onto these biomaterials from an abstract general case and reduced laboratory data, as suggested by Degueldre et al. (2001).

A potential alternative to the uranium ore mining from its classical geological formation is its extraction from seawater. Uranium is in equilibrium in seawater, as detailed in Schenk et al. (1982). This trace concentration is available at an average of 3.3 parts per billion (ppb) in standard seawater conditions of typically 35% salinity and pH 8.0 and could be extracted in a renewable mode, as per Degueldre (2016) and Degueldre et al. (2019). It would then be able to meet the needs of the world nuclear industry for many centuries to come (NEA and IAEA, 2016).

The aim of this study is to systematically simulate the sorption mechanism of uranium on biomaterial particles covered with polyphenolic groups subject to variations of pH, redox potential *E*, ligand concentrations in aqueous phase. As reported in our parent paper, McGowan et al. (2023), the methodology followed is anticipated to evaluate the surface complexation constants of all involved species by correlations as reported earlier for mono-dentate surface complexes and to additionally apply this methodology to bi-dentate surface complexes, and thus achieve the sorption study in a more complete way. In the following sections, quantification of species occurrence and of their sorption properties is introduced for the liquid and the sorbent phases.

2 Modelling species occurrence and their sorption properties

Surface complexation is the process of interactions of metal species with active surface sites of weak acid groups, which fixes the species to the surface. It is best described by the distribution ratio, which yields a distribution coefficient (K_d) quantified in mL g^{-1} for the sorption/desorption at equilibrium.

In the wet phase conditions it is convenient to include the colloidal particle concentration and to write K_d as:

$$K_d = \frac{[M]'_{sorb}}{[M]'_{Sol}} \frac{1}{[Part]} \quad (1)$$

Where both concentrations $[M]'_{sorb}$ and $[M]'_{sol}$ are given in mol mL^{-1} and [Part] is the particle concentration (e.g. g mL^{-1}).

2.1 Site availability

For the purposes of this model implementation, the particle are assumed to be spherical in nature and of fixed average radius size *r* (e.g. in nm). The chemical surface is covered by $>Su(OH)_c$ groups, with *>Su* the group substratum. The particle average surface area, *S* (e.g. nm^2) and mass m_a (g) are calculated, using ρ (g nm^{-3}) the material specific mass as described in McGowan et al. (2023).

The molecular structure is abstracted to planes on which active sorption sites are attached. The sites were assumed of rectangular shape and dimensions *a* and *b* (nm), in which there are ***c*** sites interacting with the ion or its complexes.

By considering a scaling factor, *I*, defined as the fraction of inactive surface area in the total surface area *S*. A molar site density N_s (mol per average particle surface area) is estimated by calculating the size of the interactive plane of active surface.

$$N_s = c\ S\ N_{Av}^{-1}\ a^{-1}b^{-1}(1\text{-}I) \quad (2)$$

where c is the number of active sites in the bound plane and N_{Av} is Avogadro's constant.

Total site concentration ($[>Su(OH)_c]_{Tot}$) in mol L^{-1} is then calculated using m_a, N_s and the [Part] concentration in g L^{-1}, as illustrated by Eq (3).

$$[>Su(OH)c]_{Tot} = \frac{N_s\,[Part]}{m_a} \quad (3)$$

The $[>Su(OH)_c]_{Tot}$/[Part] ratio may also be derived experimentally using for example the specific surface provided by BET measurements. Note that the site can be formulated as any valid site form, such as *>Su*, $>Su(O^-)_c$, … $>Su(OH)_c$ or any other sorption form, depending on the operating conditions.

2.2 Effect of acidity on site availability

The most common form of $[>Su(OH)_c]_{Tot}$ is $>Su(OH)_c$ as this form is function of the acidity conditions of the surrounding and the resulting number of sites of a suitable state for binding. The protonation and deprotonation of mono- active sites are accounted by specific acid/base reactions as follows.

$$>SuOH \Leftrightarrow\ >SuO^- + H^+ \quad \{1\}$$

The acid-base constant associated to these sites is defined as:

$$K_a = \frac{[>SuO^-]\,[H^+]}{[>SuOH]} \quad (4)$$

Since the total concentration of sites is defined in {1}, $[>SuOH]_{Tot}$ would be the sum of $[>SuO^-]$ and $[>SuOH]$, the protonated site concentration is expressed by:

$$[>SuOH] = \frac{\frac{[>SuOH]_{Tot}\,[H^+]}{K_a}}{1+\frac{[H^+]}{K_a}} \qquad (5)$$

In the case where a second (and a third) site is in close proximity of the first, it is possible that the surface components experience coupled acid - base reactions as defined in {1}. This reaction becomes in a general case, of multi-site reactions:

$$>Su(OH)_c \quad \Leftrightarrow \quad >Su(O^-)_c \; + \; c\,H^+ \qquad \{2\}$$

The corresponding cumulative multi-acid-base constant is given by:

$$\beta_{a(c)} = \frac{[>Su(O^-)_c]\,[H^+]^c}{[>Su(OH)_c]} \qquad (6)$$

with c= 1,2,3.

2.3 Metal hydroxide complexes

In order to define the stepwise acid/base properties of metals, it is possible to use the build-up of hydroxide complexes formed from the metal ions interacting with water, exchanging with the H+ ion to form successive hydroxide complexes, as a standardisation metric, which are formed per reaction {3}.

$$c(HOH) \; + \; M^{m+} \Leftrightarrow (HO)_cM^{(m-c)+} \; + \; c\,H^+ \qquad \{3\}$$

When equilibrium conditions are reached, the hydroxide complexation constants β_h associated to the reactions {3} are given as:

$$\beta_{\,h(c=1,2,3,4)} = \frac{[(HO)_c\,M^{(m-c)+}]\,[H^+]^c)}{[(HOH)_c][M^{m+}]} \qquad (7)$$

The net β_h of the sequential reaction from mono-dentate to bi-dentate and beyond results in Eq.(8).

$$\beta_{h(1,2,3,4)} = \prod K_{h\,1}.K_{h\,2}.K_{h\,3}.K_{h\,4} \qquad (8)$$

2.4 Correlation between mono- or multi- dentate stability constants with their respective hydroxide complexes constants.

In order for the metal or complex to react the surface of different hydrated states, the stability constant of the surface complexes K_s is estimated by correlating the hydrolysis constants K_h or β_h of the ions and complexes or the corresponding β_s involved with the surface complexation states Degueldre et al. (1994) and described by the set of reactions {4} with {5}.

$$>Su(OH)_c \; + M^{m+} \Leftrightarrow >Su(O)_cM^{(m-c)+} \; + c\,H^+ \qquad \{4\}$$

$$c\,(HOH) \; + M^{m+} \Leftrightarrow (HO)_cM^{(m-c)+} \; + c\,H^+ \qquad \{5\}$$

with

$$K_{s(c)} = \frac{[(>Su(O)c\,M^{(m-c)+}]\,[H^+]^c)}{[>Su(OH)c\,][M^{m+}]} \qquad (9)$$

The relation between {4} and {5} on the case c=1 was shown to be of the form.

$$\mathrm{Log}\, K_s = S_m \,\mathrm{Log}\, K_h + T_m \qquad (10)$$

where S_m and T_m are surface-specific constants as defined in (McGowan, et al., 2023).

However, the analysis of reactions where c>1 has shown that successive multi-dentate relations have the same form as (10), as long as constant c matches.

Several authors have shown that the multi-dentates are common for uranium e.g., Carbonaro et al. (2011). High S_m and low T_m values, respectively, were reported by Pontoni et al. (2022) for details.

2.5 Complexes formation in the redox range

The hydrolysis stability constants of both redox species ($K_{s,i,k}$ for oxidising and $K_{s\,j,l}$ for reducing species) can be obtained by evaluating the stepwise iterations of reaction {2}. It should be noted that the notation is intended to include both oxo- and non-oxo- cation species.

Further complicating situation is the interference originating from the metal complexation by *k*-ligands or *l*-ligands (L^{p-}) such as carbonates. The indices are ranged over the co-ordination properties of the appropriate element, as illustrated in Fig. 1.

$$MO_x(\mathrm{OH})_{i-1}L_k{}^{z-2x-n-i+1-kp} + \mathrm{H_2O} \overset{K_{s,i,k}}{\Longleftrightarrow} MO_x(\mathrm{OH})_i L_k{}^{z-2x-n-i-kp} + \mathrm{H^+} \quad \{6\}$$

$$MO_y(\mathrm{OH})_{j-1}L_l{}^{z-2y-n-j+1-lp} + \mathrm{H_2O} \overset{K_{s,j,l}}{\Longleftrightarrow} MO_y(\mathrm{OH})_j L_l{}^{z-2y-n-j-lp} + \mathrm{H^+} \quad \{7\}$$

Therefore, it is possible to define the generalised redox couple $MO_x{}^{(z-2x)+}/MO_y{}^{(z-n-2y)+}$ (where $MO_x{}^{(z-2x)+}$ is the oxidised species and $MO_y{}^{(z-n-2y)+}$ the reduced one), as reaction {8} & {9} (see Fig. 1).

The surface complexation for the hydrolysed (and complexed) species is described (reactions {4}) by considering the generalised quasi-neutral site >*Su*$(\mathrm{OH})_c$. The surface complexation constants are $K_{s,l,k}$ for the oxidising species and $K_{s,j,l}$ for the reducing species. As stated earlier, the indices *k* and *l* refer to the appropriate co-ordination number of the metal ions, in the context of those of the selected ligand.

Fig. 1: Combined mechanisms of surface complexation and redox reaction of uranium hydroxide and carbonate complexes in solution. In this study >*Su*$(\mathrm{OH})_c$ is the *c*-hydroxy-aromatic substrate and *c*=*c'*.

Furthermore, effects of the redox potential at the surface were also taken into account (reactions {10} and {11}). The combined mechanisms of surface complexation and redox of uranium hydroxide- and carbonate- complexes in solution are depicted in Fig. 1. When the reactions are written in terms of free metal M^{z+}, the cumulative constants are $\beta_{s\,i}$ and $\beta_{s\,j}$ respectively.

By applying the Nernst equation to these, as detailed in Alonso and Degueldre (2003), the equilibrium K_d was calculated using for the mono-dentate. To extend this to account for *c* dentate bonds, it becomes (11) below, replacing [Part] per rearranged Eq (3).

$$K_d = \frac{\{\sum_{i,k}\left[\frac{K_{s,i,k}\cdot\beta_{h\,i,k}\cdot[L_k]^k}{[H^+]^i}\right] + \sum_{j,l}\left[\frac{K_{s,j,l}\cdot\beta_{h\,jl}\cdot[L_l]^l}{[H^+]^j}\right]\exp(A)\}\cdot\frac{[>SuOH]}{[H^+]^c}}{\{\sum_{i,k}\left[\frac{\beta_{h\,i,k}\cdot[L_k]^k}{[H^+]^i}\right] + \sum_{j,l}\left[\frac{\beta_{h\,j,l}\cdot[L_l]^l}{[H^+]^j}\right]\cdot\exp(A)\}\cdot[\text{Part}]} \qquad (11)$$

where $A = \frac{(E'^{\circ}-E)n\mathrm{F}}{\mathrm{R}T}$ and all concentrations are molar units unless noted otherwise.

Since K_d is proportional to the $[>Su(OH)_c]_{Tot}/[Part]$ ratio, it is proportional to 1/r.

The formulation of Eq (11) implies linear adsorption isotherms; no saturation effects, no electrostatic effects and no activity corrections at this stage.

Any K_d calculated on this basis is one instance of binding metal or complex, in the conditions specified by the E'° (apparent standard redox potential) used for A, and the appropriate β_h and K_s for that complex. Therefore, by using different corresponding conditions, K_d value can be calculated for each appropriate state at any specific value of E.

Equation (10) can be further extended to consider sorption by different multi-dentate complexes, and by using the appropriate cumulative total (β for bi-dentate). For the multi-dentate complexes the formulation is similar however c protons are exchanged instead of 1.

Finally, for the shift from U(IV) to U(VI) during increase of E, the Log Kd = f(E) curve undergoes a change of Log K_d values corresponding to the redox state change of the sorbing species. It implies an inflection in the curve characterised by $\partial^2(\mathrm{Log}K_d)/_{\partial E^2} = 0$ for a potential value called here E"°.

The following assumptions were made for the application of the proposed model:

- The surface complexation reactions occur under equilibrium.
- There are no kinetics effects considered.
- The sorption isotherms are of Langmuir type.
- The model applies to pure surface complexation with no change in charge effect from the equilibrium (for example, no double layer effect).
- There is no reaction coupling that could lead to irreversible sorption e.g. surface complexation & aggregation.

The model would be arranged accordingly in case of the sorption is also driven by these conditions.

Extension to the case of multi surface complex may be sketched by the reaction:

$$>Su'(OH)_c + >Su(O)_cM^{(m-c)+} \Leftrightarrow (>Su(O)_cM(O)_c\,Su'<)^{(m-2c)+} + c\,H^+ \qquad \{12\}$$

in the bi-ligand complex production, e.g. from two particles, with

$$K_{s(c,2)} = \frac{[(>Su(O)c\,M(O)cSu<)^{(m-'2c)+}]\,[H^+]^c)}{[>Su(OH)c\,][>Su(O)cM^{m+}]} \qquad (12)$$

This last equation cannot be used to estimate a K_d because the M^{m+} ion is blocked between two particles that makes reaction {12} irreversible as discussed in Section 5.

3. Data for model Application

3.1 Liquid environmental context

As the model is intended to represent sorption of uranium in saline conditions, the concentration of uranium was taken as the average seawater value is $3x10^{-9}$ g L^{-1} (3 ppb) as reported by Millero (2013). The pH of seawater directly used for calculations is around 8.0. For example, as reported by Rérolle et al. (2012), Irish Sea seawater has a pH between 7.995 and 8.210 and a redox potential of about +0.4 V in surface conditions.

The molecular weight of uranium is assumed to be 238 g mol^{-1}. The pK_h for each of its hydroxide complexes and the E° for each of its redox couples are as listed in Table 1.

Table 1: Hydrolysis constants and standard redox potentials of uranium (NEA (2004) and Grenthe et al. (2006))

i or j	pK_h U(III)	E° (V)	pK_h U(IV)	E° (V)	pK_h U(V)	E° (V)	pK_h U(VI)	E° (V)
=1	6.80	0	0.54	-0.553	0.00	0.053	0.00	0.006
=2	7.30	0	0.70	-0.553	11.30	0.053	5.25	0.006
=3	11.60	0	3.60	-0.553	12.30	0.053	6.90	0.006
=4	14.35	0	5.30	-0.553			8.10	0.006
=5			13.10	-0.553			12.15	0.006

For the carbonated seawater environment, the total carbonate concentration has been assumed to be $[CO_3]_{Tot} = 2.2 \times 10^{-3}$ mol L^{-1} and their first and second Log partition coefficients are 10.329 and 16.681 (Sharp et al. (2017)). The pK_h for each of the hydrolysis constants and *E*° (V) are listed in Table 2 and ranked over an order that follows the number of carbonating- ligands.

Table 2: Hydroxide complex constants and standard redox potentials of uranium carbonated states data from NEA (2004) and Grenthe et al. (2006).

i & l (for $K_{i,l}$)	pK_h U(III)	E° (V)	j & l (for $K_{j,l}$)	pK_h U(IV)	E° (V)
i=0, l=1/ 2/ 3	5.12 /1.80 / -1.90	0	j=0, l=1/ 2/ 3/ 4	6.5/ 5.3/ 1.6/ -3.4	-0.553
i= 1, l=0	-11.3	0	j= 1, l=0/1/2	-6.8 /-5.8 /-7.8	-0.553
i= 2, l=0	-12.3	0	j= 2, l=0/1	-7.3/ -7.9	-0.553
			j= 3, l=0	-11.6	-0.553
			j= 4, l=0	-14.35	-0.553

j & l (for $K_{j,l}$)	pK_h U(V)	E° (V)	j & l (for $K_{j,l}$)	pK_h U(VI)	E° (V)
j=0, l=1/ 2/ 3/ 4	13.7/ 10.6/ 7.6/ 3.3	0.053	j=0, l=1/ 2/ 3/ 4	9.94/6.67/ 5.23/7.6/ 3.3	0.006
j= 1, l=0	-0.54	0.053	j= 1, l=0	-5.25	0.006
j= 2, l=0	-0.7	0.053	j= 2, l=0	-6.9	0.006
j= 3, l=0	-3.6	0.053	j= 3, l=0	-8.1	0.006
j= 4, l=0	-5.3	0.053	j= 4, l=0	-12.15	0.006
j= 5, l=0	-13.1	0.053			

3.2 Sorbent environmental context: phenolic phases

A review of stability constant data for solid phase phenolic acids with d and f block metal ions has been carried out, considering hydroxy-benzene, the (1,2) and the (1,3) isomers of dihydroxy-benzene, and the (1,3) isomer of dihydroxy-naphthalene. The (1,4) isomer was of dihydroxy-benzene but the data was insufficient to make a correlation. In practice, the (1,2) and (1,3) isomers of dihydroxy-benzene proved to be co-linear: and the data was combined to increase the dataset accuracy.
Due to the ranging of source data used to compute the relations, testing error was not considered as the sources do not follow a consistent methodology. The reported values span a (narrow) range of testing conditions (Martell and Smith (1989)). Most values reported for stability constants and hydrolysis constants were tested at 25 °C, but some variations which varied between 18°C and 32°C were included. More ranging variability stem from the range of ionic strength of solution, which would lead them to be distinct from the basis used for the hydrolysis constant. In cases where corresponding conditions were found unavailable, an interpolated value was computed from those that were available possible or discounted otherwise. This variability is only reported for the final T_m and S_m variance for simplicity.

Furthermore, data on multi-dentate interactions are limited, with data available for the mono- and bi-dentates of dihydroxy-benzene, and mono- only for the other two. This is likely not directly relevant in practice, as this effect results from the product compounds being too unstable to have detectable residence times in solution. This has limited the calculated T_m and S_m to the mono form, especially since dihydroxy-benzene was found of collinear trend and the reported values would be indistinguishable at the reported precision.

Fig. 1. Comparison of various phenolic complexation constants and hydroxide complexation constants of various metal ions, in mono-dentate (1:1) and bi-dentate (1:2) binding, data from Martell and Smith (1989).

For the purposes of mapping the relationship, the -Log of the hydrolysis constant was compared to the -Log of the stability constant. It showed that the relationship is linear with all trend line fits, exhibiting an R^2 greater than 0.85. Relationships between the different forms are rather evident. The mono- and the bi- dentate forms of dihydroxy-benzene are almost fully co- linear with the small discrepancy, likely due to measurement error. Although there is only very limited data available, dihydroxy-naphthalene also exhibits a very similar S_m. Additionally, the S_m of the mono-hydroxy-benzene form is approximately half that of the dihydroxy-aromatic form, suggesting a strongly fixed relation. These are

displayed in Table 3. The minimum energy threshold T_m exhibits the primary difference between forms. These are displayed in Table 3. The confidence interval of the data set from the plotted correlation reported in Fig 2 is also displayed in this table, for information.

Although not displayed due to lack of data, data for (1,4) dihydroxy-benzene had a T_m value similar to the displayed dihydroxy- form, but a value of S_m which is consistent with the mono-hydroxyl form, supports the hypothesis suggested above. This relation therefore is assumed to hold for the other phenolics.

In order to make the work relevant to our ongoing experimental work, the sorbent materials were assumed to consist of spherical particles 0.2 mm in diameter, with a total concentration of 30 g L^{-1}, Ref.: McGowan et al (2022). The characteristics of each of the three are listed in Table 3 and the values are based on standard temperature (25°C) and pressure (1 Atm) where appropriate.

Table 3. Material property values used for the simulation.

	a (nm)	*b* (nm)	*c* (-)	Density (g cm^{-3})	Molar Mass (g)	pKa
Hydroxy-benzene	0.43	0.57	1	1.07	94.11	9.99
(1,2) and (1,3) dihydroxy-benzene	0.55	1.01	2	1.34	154.21	9.45
(1,2) dihydroxy-naphthalene	1.1	1.0	2	1.30	160.17	9.04
	T_m (c:1//2)	S_m (c:1//2)	Confidence interval +/-	Site Density (nm^{-2})	$[>SuOH]_{Tot}$ ($mol.g^{-1}$)	
Hydroxy-benzene	-1.85/-1.85	0.85/0.85	1.86	4.08	9.50E-08	
(1,2) and (1,3) dihydroxy-benzene	2.56/2.56	1.54/1.56	0.60/2.00	3.61	3.35E-08	
(1,2) dihydroxy-naphthalene	-8.15/-8.15	1.48/1.48	5.19	1.80	1.73E-08	

4.0 Results

4.1 Speciation of uranium in water, effect of pH, E and carbonate complexes

In aqueous environment uranium can form tetravalent, pentavalent and hexavalent species, where the stability domains can be recurrently calculated as a function of pH and E for given ligand concentrations. The E vs pH diagrams for uranium were replotted, as reported in Degueldre and McGowan (2020). Results are presented in **Fig. 3a&b**.

Uranium hexavalent in water exists primarily as ionic as well as carbonate and hydroxide complexes. In seawater uranium (oxidising), carbonate complexes are often found bound to calcium ions. In order of prevalence, these are tri-carbonate-uranyl [$UO_2(CO_3)_3^{4-}$] (as the dominant form, constitutes 84.9% of all free uranium), di-carbonate-uranyl [$UO_2(CO_3)_2^{2-}$], uranyl (VI) tri-hydroxide [$UO_2(OH)_3^-$], uranyl [UO_2^{2+}], uranyl hydroxide [$UO_2(OH)^+$], and uranyl di-hydroxide [$UO_2(OH)_2$] as reported by Djogic and Branica (1993), Zhang et al. (2005), Sekiguchi et al. (1994), Aihara et al. (1992) and Yamashita et al. (1980).

In reducing seawater conditions, uranium forms trivalent species which are at pH8 mainly uranium tetra-hydroxide [$U(OH)_4$], along with some uranium tri-hydroxide [$U(OH)_3^-$]. The carbonate complexes are absent under these pH – E conditions.

Fig. 2. Indicative uranium E'° – pH plots for **a**. carbon free and **b.** carbonated solutions ($[CO_3]_{Tot}$ = $2.2x10^{-3}$ mol L^{-1}) solutions. Note the oxidising (+0.4 V for sea water) and reducing (e.g. -0.4 V for phenolic couple) domain are depicted.

4.2 Calculated K_d, effect of pH and E for polyhydroxy-aromatic group complexes

4.2.1 Calculation of K_d for hydroxy-benzene group complexes

Effect pH and E

The K_d (mL g^{-1}) for uranium surface complexation by hydroxy-benzene groups on bioorganic particles in a carbonate free environment, and a $[CO_3]_{Tot}$ = 2.2 x 10^{-3} mol L^{-1} carbonated environment as a function of redox potential for various pH values was first calculated. The surfaces of the particles of 0.2 mm size are covered by hydroxy-benzene groups forming multi dentate complexes with U(VI) and at lower E values U(IV). In this case, calculations were done using the correlations with T_m and S_m given in Table 5. The results are plotted in **Fig. 4a&b**.

Fig. 3 Uranium sorption coefficient K_d (mL g^{-1}) as a function of potential for various pHs on multi-dentate (hydroxyl-benzene) group loaded particles. Conditions: particles of 0.2 mm size, potential vs NHE, bidentate c= 2, site density: 4.1 nm^{-2}, for site parameters see Table 3.
a. Carbonated: ($[CO_3]_{Tot}$ = 2.2 x 10^{-3} mol L^{-1}) and **b.** carbonate free: $[CO_3]_{Tot}$ = 0 mol L^{-1})

The general form of the distribution is three distinct phases. Two of these are stable states, where the Log K_d is dominated by U(VI) and U(VI) complexes, respectively. In between the two phases there is

a transition phase, which is characterised by a gradual change in dominant complex, from U(IV), to U(V)/U(VI) and to U(VI) forms. The U(V) concentration does not become significant under these conditions. This transition phase is defined by the two *E* (V) where the stable state starts to drift Log K_d.

With hydroxy-benzene, the U(IV) form occurs outside the water stability zone, and therefore it is only theoretical value. In many cases, the transition phase is also outside this region. The exception is the pH 4 form, where the U(III) has a significant effect at very low E (V). However, this is also outside the water stability zone. Without the presence of ligands, the trend is found the same, but the balance is reversed, with the U(VI) form exhibiting higher K_d. The exception is again at pH 4, where the higher zone is the U(IV) phase. These values are displayed in the Table 4.

Table 4. Calculated characteristics of the K_d of hydroxy-benzene (as per Fig. 4)

pH	Log K_d U(IV)	Log K_d U(VI)	U(IV) limit (V)	U(VI) limit (V)	Water Stability (V)
4	-20.16	-18.00	-0.22	-0.02	>-0.24
6	-8.20	-9.94	-0.52	-0.29	>-0.36
8	+3.79	-0.70	-0.88	-0.59	>-0.48
10	+9.99	+8.1	-1.07	-0.92	>-0.60
pH (CO_3 free)					
4	-2.83	-4.16	-0.26	-0.09	>-0.24
6	+2.52	+3.07	-0.46	-0.31	>-0.36
8	+6.59	+9.05	-0.74	-0.51	>-0.48
10	+9.99	12.82	-1.09	-0.80	>-0.60

Effect of total carbonate concentration

The K_d (mL g^{-1}) for uranium surface complexes by hydroxy-benzene groups on bioorganic particles was calculated in carbonate solutions which $[CO_3]_{Tot}$ ranges from 2.2 x 10^{-6} to 2.2 mol L^{-1}, as a function of the redox potential for pH 8.0. This range was selected as it reflects an order of magnitude on each side of the recorded concentration at depth in the Irish Sea (Rérolle, et al. (2012) [xix]). The surfaces of the particles of 0.2 mm size are covered by hydroxy-benzene groups, forming multi-dentate complexes with U(VI) and at lower E values U(IV). The Calculations were first completed using the correlations with T_m and S_m given in Table 5. The results are presented in **Fig. 5**.

Fig. 4 Uranium sorption coefficient K_d (mL g^{-1}) as a function of potential for pH 8.0 on mono-hydroxy-benzene group loaded particles. Conditions: particles of 0.2 mm size, potential vs NHE, bidentate c= 2, site molecular characteristics per Table 3, over varying $[CO_3]_{Tot}$.

In general, increasing the CO_3^{2-} concentration decreases the sorption of U ions, which is to be expected, since carbonate acts as an interfering ligand. The interference effect on U(IV) is lower than the effect on the U(VI) complexes, so the transition step seen in Fig. 4 is also in evidence. The exceptions are the carbon free curve and the concentration of 2.2 x 10^{-6} mol L^{-1} where the stronger bonding of the U(VI) can win out, without presence of the interfering ligand. The entry point for the transition varies but the

limiting point is always about -0.6 V, although at low concentrations, the pH effect on the solubility of the CO_3^{2-} causes a small degree of variation.

At pH 8, in practice, the transition is below the water stability region, so values for U(IV) follow theoretical ones.

Table 5. Calculated properties of the K_d of hydroxy-benzene at pH 8 in varying $[CO_3]_{Tot}$ other conditions see Fig. 4

$[CO_3]_{Tot}$ (M)	Log K_d U(IV)	Log K_d U(VI)	U(IV) limit (V)	U(VI) limit (V)
$0x10^{1}$	+6.59	+9.05	-0.74	-0.54
$2.2x10^{-6}$	+6.59	+7.69	-0.74	-0.58
$2.2x10^{-5}$	+6.59	+5.20	-0.79	-0.62
$2.2x10^{-4}$	+6.52	+2.29	-0.87	-0.61
$2.2x10^{-3}$	+3.79	-0.70	-0.88	-0.61
$2.2x10^{-2}$	-0.13	-3.70	-0.85	-0.61
$2.2x10^{-1}$	-4.13	-6.70	-0.81	-0.61
$2.2x10^{0}$	-8.18	-9.70	-0.78	-0.61

4.2.2 Calculation of K_d for dihydroxy-benzene group complexes

Effect pH and E

The K_d (mL g^{-1}) for uranium surface complexation by dihydroxy-benzene groups on bioorganic particles in a carbonate free environment, and carbonated ($[CO_3]_{Tot}$ = 2.2 x 10^{-3} mol L^{-1}) as a function of redox potential for various pH values was first calculated. The surfaces of the particles of 0.2 mm size are covered by phenolic groups forming multi-dentate complexes with U(VI) and at lower E values U(IV). In this case, the calculations were carried out using the correlations for T_m and S_m given in Table 5. The results are plotted in **Fig. 6a&b**.

Fig. 5 Uranium sorption coefficient K_d (mL g^{-1}) as a function of potential for various pHs on multi-dentate phenolic (dihydroxy-benzo-) group loaded particles. Conditions: particles of 0.2 mm size, potential vs NHE, site density: 3.6 nm^{-2}, bidentate c= 2, **a**. carbonate free, **b**. carbonated $[CO_3]_{Tot}$ = $2.2x10^{-3}$ mol L^{-1}).

As with the mono-hydroxybenzene, the general form of the distribution shows three distinct phases. Two of these are stable states, where the Log K_d is dominated by U (VI) and U (VI) complexes, respectively. In between the two phases, there is a transition phase which is characterised by a gradual change in dominant complex, from U(IV) , to U(V)/U(VI), to U(VI) forms. The U(V) form does not become significant under these conditions, which means the transition follows a linear trend. This transition phase is defined by the two E (V) where the stable state starts to drift from the stable Log K_d.

For the ligand free results, the U(VI) zone has a higher K_d than the U(IV) zone, except for pH 4. This trend is mostly reversed for the carbonated environment except for pH 10, where the transition is minor but in the other direction, due to the basic conditions interfering with the carbonate solubilty. In general, the transition zone is outside the stable water zone, so the values for the U(IV) are theoretical ones. The exception is at pH 4, where the transition zone is at a similar E (V) as the U(IV) transition point.

Table 6. Calculated characteristics of the K_d for dihydroxy-benzene complexes

pH (CO_3)	Log K_d U(IV)	Log K_d U(VI)	U(IV) limit (V)	U(VI) limit (V)	Water Stability (V)
4	-15.02	-11.61	-0.26	-0.05	-0.24
6	-03.03	-03.10	-0.49	-0.31	-0.36
8	+08.97	+06.74	-0.88	-0.69	-0.48
10	+15.59	+16.61	-1.11	-0.95	-0.60
pH (0-CO_3)					
4	+02.31	+02.24	-0.24	-0.18	-0.24
6	+07.70	+09.90	-0.51	-0.33	-0.36
8	+11.77	+16.48	-0.81	-0.55	-0.48
10	+15.59	+20.72	-1.11	-0.83	-0.60

Effect of total carbonate concentration.

The K_d (mL g^{-1}) for uranium surface complexation by dihydroxy-benzene groups on bioorganic particles was calculated in a carbonate suspensions where $[CO_3]_{Tot}$ varies between 2.2 x 10^{-6} and 2.2 mol.L^{-1} as a function of redox potential for pH 8.0. This range was selected as it reflects an order of magnitude on each side of the recorded concentration at depth in the Irish Sea (Rérolle, et al., 2012). The surfaces of the particles of 0.2 mm size are covered by dihydroxy-benzene groups forming multi-dentate complexes with U (VI) and at lower E values U (IV). The calculations were completed using the correlations with T_m and S_m given in Table 5. The results are plots are plotted in **Fig. 7**.

Fig. 6 Uranium sorption coefficient K_d (mL g^{-1}) as a function of potential for pH 8.0 on multi-dentate group loaded particles. Conditions: particles of 0.2 mm size, potential vs NHE, characteristics per Table 3, over varying carbonate concentrations

In general, increasing the $[CO_3]_{Tot}$ decreases the sorption of U ions, which is to be expected, since it is an interfering ligand. The interference effect on U(IV) is lower than the effect on the U(VI) complexes, so the transition step seen in Fig. 5 is also in evidence. The limiting point for U(IV) transition varies, but the limit potential for U(VI) is always about -0.80 V. It is notable that in comparison to the mono-hydroxy-benzene, for the $[CO_3]_{Tot}$ 10^{-5} mol L^{-1} and below, the interfering effect of the U(VI) form is insufficient to counteract the increased bonding potential of that form, compared with the U(IV) form, but at the highest concentration, this repeats, as the suppressive effect on the U(IV), form is higher.

At pH 8, in practice, the transition is below the water stability region, so values for U(IV) are mostly theoretical, except some results close to the limiting point.

Table 7. Calculated characteristics of the K_d for dihydroxy-benzene at pH 8 in varying $[CO_3]_{Tot}$

$[CO_3]_{Tot}$ (M)	Log K_d U(IV)	Log K_d U(VI)	U(IV) limit (V)	U(VI) limit (V)
$0.0x10^{1}$	+13.18	+17.90	-0.80	-0.55
$2.2x10^{-6}$	+13.18	+16.54	-0.80	-0.59
$2.2x10^{-5}$	+13.18	+14.05	-0.80	-0.67
$2.2x10^{-4}$	+13.11	+11.14	-0.87	-0.69

$2.2x10^{-3}$	+10.38	+08.15	-0.88	-0.69
$2.2x10^{-2}$	+06.42	+05.15	-0.86	-0.69
$2.2x10^{-1}$	+02.47	+02.15	-0.81	-0.70
$2.2x10^{0}$	-01.58	-00.85	-0.79	-0.66

448

449 **4.2.3 Calculation of K_d for dihydroxy-naphthalene group complexes**

450 ***Effect pH and E***

451 The K_d (mL g^{-1}) for uranium surface complexation by dihydroxy naphthalene groups on bioorganic
452 particles in a carbonate free environment, and in a carbonated environment ($[CO_3]_{Tot}$ = 2.2 x 10^{-3}
453 $mol.L^{-1}$) as a function of redox potential for various pH values was first calculated. The surfaces of the
454 particles of 0.2 mm size are covered by phenolic groups, forming complexes with U(VI) and at lower
455 E values U(IV). In this case calculations were done using the correlations with T_m and S_m given in
456 Table 5. The results are plotted in **Fig. 8**.

457

458

459 **Fig 7** Uranium sorption coefficient K_d (mL g^{-1}) as a function of potential for various pHs on
460 dihydroxy-naphthalene group loaded particles. Conditions: particles of 0.2 mm size, potential vs
461 NHE, site density: 1.8 nm^{-2}, bidentate c= 2,

462

463 As with the previous forms, the general form of the distribution represents three distinct phases. Two
464 of these are stable states, where the Log K_d is dominated by U (VI) and U (VI) complexes respectively.
465 In between the two phases, there is a transition phase, which is characterised by a gradual change in
466 dominant complex, from U(IV) , to U(V)/U(VI), to U(VI) forms. The U(V) form does not become
467 significant under these conditions, which means the transition is of linear trend. This transition phase is
468 defined by the two E (V) where the stable state starts to drift from the stable Log K_d. The transitions for
469 this surface are of much softer changes than the other forms.

470 In the carbon free form, as discussed earlier, the U(VI) form is dominant, except for pH 4. With the
471 carbonated form, this is reversed, except for at pH 10, where the interference effect is minimized and
472 the U(VI) phase is higher. In general, the transition zone is outside the stable water zone, so the values
473 for the U(IV) are theoretical ones. The exception is at pH 6, where the transition zone is at a similar
474 E(V) as the transition point, and pH 4, where it precedes it. The U(IV) limiting point is consistent
475 between the two, but the U(VI) limiting point varies less consistently.

476

Table 8. Calculated characteristics of the K_d of di-hydroxy-naphthalene

pH Carbonated	Log K_d U(IV)	Log K_d U(VI)	U(IV) limit (V)	U(VI) limit (V)	Water Stability (V)
4	-25.09	-21.84	-0.26	-0.03	-0.24
6	-13.09	-13.34	-0.52	-0.37	-0.36
8	-01.17	-03.57	-0.87	-0.65	-0.48
10	+03.80	+04.65	-01.10	-0.92	-0.60
pH (C free)					
4	-07.75	-08.00	-0.27	-0.12	-0.24
6	-02.37	-00.34	-0.51	-0.30	-0.36
8	+01.63	+06.17	-0.81	-0.51	-0.48
10	+03.80	+08.76	-1.10	-0.80	-0.60

Effect of total carbonate concentration

The K_d (mL g^{-1}) for uranium surface complexation by a dihydroxy-naphthalene group on bioorganic particles was calculated in carbonate solutions which $[CO_3]_{Tot}$ varies between 5 x 10^{-4} and 6 x 10^{-3} mol L^{-1} as a function of redox potential for pH 8.0. This range was selected as a reasonable proximity for surface carbonate concentrations in the Irish Sea (Rérolle, et al. (2012) [xix]). The surfaces of the particles of 0.2 mm size are covered by dihydroxy-naphthalene groups forming multi-dentate complexes with U(VI) and at lower E values U(IV). The calculations were first done using the correlations with T_m and S_m given in Table 5 for mono-dentate. The results are plotted in **Fig. 9.**

Fig 8 Uranium sorption coefficient K_d (mL g^{-1}) as a function of potential for pH 8.0 on dihydroxy-naphthalene group loaded particles. Conditions: particles of 0.2 mm size, potential vs NHE, characteristics per Table 3, over varying carbonate concentrations

As the carbonate concentration increases, the interference effect in the complex formation proportionately increases. Below concentrations of 2.20x10^{-5} mol L^{-1}, the effect on the U(IV) Log K_d is negligible, with a value of +1.63. Above this concentration, the U(IV) Log K_d is reduced. The U(VI) phase would also be decreasing with increasing carbonate concentration, although the effect is not as significant as that during the U(IV) dominated phase.

Table 9. Calculated characteristics of the K_d of dihydroxy-naphthalene at pH 8 in varying $[CO_3]_{Tot}$

$[CO_3]_{Tot}$ (mol L^{-1})	Log K_d U(IV)	Log K_d U(VI)	U(IV) limit (V)	U(VI) limit (V)
0.0x10^{+1}	+01.63	+06.17	-0.81	-0.55
2.2x10^{-6}	+01.63	+04.81	-0.81	-0.60
2.2x10^{-5}	+01.63	+02.33	-0.81	-0.63
2.2x10^{-4}	+01.56	-00.58	-0.86	-0.69
2.2x10^{-3}	-01.17	-03.57	-0.87	-0.68
2.2x10^{-2}	-05.09	-06.57	-0.84	-0.68
2.2x10^{-1}	-09.08	-09.57	-0.84	-0.69
2.2x10^{0}	-13.13	-12.57	-0.79	-0.67

5 Discussion.

As expected, the sorption (Log K_d) increases together with the pH. This is due to the deprotonation of the hydroxy-aromatic groups. From the redox point of view, the reduction from U(VI) species in U(IV) species appears when decreasing E. Equation (12) demonstrates clearly that K_d is proportional to the inverse of the particle sizes. This allows to increase the sorption coefficient by reducing the size of the particles.

Competition by sorption with other elements is not treated here because the concentration of strongly sorbing elements is at least 2 orders of magnitude below that of uranium, e.g. lanthanides, Th and Pb), the sorbing tracers such as Mn, Ni, Cu are about 1 order of magnitude below uranium, other elements such as Mg, Ca, Sr and Ba sorb more by ion exchange processes.

In addition when multi-particulate complexation takes place such as sketched in reaction {12}, multiple reactions (e.g. H- bridging after double surface complexation) completing the simple surface complexation take place. In these conditions surface complexation involves also additional reactions that makes this surface complexation more complicated yielding an aggregate in which the metal ion escapes from is potential de-complexation making the process irreversible. In this context the K_d concept is not anymore valid. In the cases discussed below, only surface complexation takes place in the sorption process.

5.1 Variation between the hydroxy-aromatic systems.

In general, the three polyhydroxy-aromatic cases (Section 4.2-4) follow the same pattern (Log K_d = f(E)) and have relatively narrow width (ΔE) of their transition phases between the U(VI) and the U(VI) forms (between 0.06 and 0.30 V), see Table 10 and (Fig. 4, 6 & 8). All the transition points are similar between the materials, varying only over the order of 0.05 V. Except for the pH 6 curve where the mono-hydroxy-benzene has a reduced U(VI) limit for the carbonated curves, compared to the other two, where this variation is ~0.1 V. This is due to relatively weak concentration of U(V) forms under these conditions, which leads to a reduced transition to the U(VI) dominated phase, while the other curves experience a longer transition.

Table 10: Redox potential width (ΔE) for the U(IV)/U(VI) transition on the Log K_d plots.

	Δ Log K_d (mL g^{-1})			**ΔE (V)**		
pH	**Mono-hydroxy-benzene**	**Di-hydroxy-benzene**	**Di-hydroxy-naphthalene**	**Mono-hydroxy-benzene**	**Di-hydroxy-benzene**	**Di-hydroxy-naphthalene**
4	**+2.16**	**+3.41**	**+3.24**	**0.20**	**0.21**	**0.29**
6	**-1.73**	**-0.07**	**-0.25**	**0.23**	**0.09**	**0.15**
8	**-4.49**	**-2.23**	**-2.40**	**0.29**	**0.19**	**0.22**
10	**-1.29**	**+1.02**	**+0.85**	**0.18**	**0.16**	**0.18**
pH (CO_3 free)						
4	**-1.33**	**-0.07**	**-0.25**	**0.17**	**0.06**	**0.15**
6	**+0.55**	**+2.20**	**+2.03**	**0.14**	**0.18**	**0.21**
8	**+2.46**	**+4.71**	**+4.54**	**0.23**	**0.26**	**0.30**
10	**+2.83**	**+5.13**	**+4.96**	**0.29**	**0.28**	**0.30**

The transitions for the carbon free curves themselves are negative for pH 4 curve and positive for the pH 6-10 curves, while Log K_d = f(E) transitions for the carbonated case are negative for the pH 4 and 10 curves, and positive for the pH 6 and 8 curves.

The exceptions to this are mono-hydroxy-benzene, where the step changes are positive for pH 10. This is due to the interference effect of the site acidic form on the low pH curves and the reduced effect on sorption by the carbonate at high pH. The lower site density for the mono-hydroxy-benzene means it is not as suppressed by the carbonate as in the di-hydroxy forms.

Of the three substrates, the mono- form displays exceptional differentiation in the transitions. Whereas the bi-forms display broadly similar height changes at the same pH, the mono form follows a different pattern, with the effect of pH change on the separation between the U (IV) and U (VI) stable states being maximised at low pH. Increasing the pH in the mono form increases the K_d in the carbon free system, but decreases it in the carbonated system, although the step change effect is maximised for the pH 8 curve, with the height change for pH 10 being reduced.

Considering the three under the curve closest to natural conditions mentioned previously (pH 8.0, a potential of 0.4 V), the mono- -benzene form would estimate at 5.6, the di-hydroxy- forms are 14.6 and 3.2 respectively. To adjust these to allow IV dominance, these would require a shift of over -1 V for all three. This would require a two electron redox shift to achieve (Lambert, et al. 2020)[[i]] . This is possible but unlikely to occur at the specified pH. However, in the context of a pH drop to 6.0, such as could occur during fermentation, a shift of only -0.8 V (which would correspond to a single electron redox shift), would be possible.

5.*2* Variation with the carbonate concentration.

In the presence of carbonate ligands, the competition effects from the carbonates are noticeable (see Table 11). Below $[CO_3]_{Tot}$ =2.2 x 10^{-5} M, the interfering effect on the U(IV) phase is insignificant, but rapidly increases until there is little difference between it and the U(VI), which experiences a continually increasing interfering effect at any concentration. This would most likely be due to the stereochemistry effects limiting the return to solution of the U(IV), while the U(VI) carbonate complex is stronger, allowing rerelease if a carbonate interacted. In all three cases, the change between the two redox phases decreases from the positive Log K_d for $[CO_3]_{Tot}$ of 0 mol L^{-1}, down to a maximum negative value. The di forms mirror each other, but interestingly separation occurs for surface seawater conditions (2.2x10^{-3} mol L^{-1}).

Table 10. Calculated characteristics of the Log K_d changes between redox states for varying CO_3 for the three aromatic groups

	Δ Log K_d (mL g^{-1})			**ΔE (V)**		
$[CO_3]_{Tot}$ (mol L^{-1})	**Mono-hydroxy-benzene**	**Di-hydroxy-benzene**	**Di-hydroxy-naphthalene**	**Mono-hydroxy-benzene**	**Di-hydroxy-benzene**	**Di-hydroxy-naphthalene**
0.0x10^{+1}	**+2.46**	**+4.72**	**+4.54**	**0.20**	**0.28**	**0.26**
2.2x10$^{(-6)}$	**+1.10**	**+3.36**	**+3.18**	**0.16**	**0.23**	**0.21**
2.2x10$^{(-5)}$	**-1.39**	**+0.87**	**+0.70**	**0.17**	**0.15**	**0.18**
2.2x10$^{(-4)}$	**-4.23**	**-1.97**	**-2.14**	**0.26**	**0.18**	**0.17**
2.2x10$^{(-3)}$	**-4.49**	**-2.23**	**-2.40**	**0.27**	**0.19**	**0.19**
2.2x10$^{(-2)}$	**-3.57**	**-1.31**	**-1.48**	**0.24**	**0.16**	**0.16**
2.2x10$^{(-1)}$	**-2.57**	**-0.32**	**-0.49**	**0.20**	**0.18**	**0.15**
2.2x10$^{(0)}$	**-1.52**	**+0.73**	**+0.56**	**0.17**	**0.13**	**0.12**

5.3 Comparison of results with experimental data

Comparing the values gained by applying the model with experimental data is challenging, as natural polyphenolics are often resonant and produced by under race conditions by dynamic systems, leading to picking out specific structures is next to impossible. This is why this model has been aimed towards representing a median structure, whose values can be used to direct by values to mirror the real-world comparisons.

For example, Yu et *al*. (2022) combined titanium oxide and bayberry tannins to form particles with capture rates peaking at base concentration corresponding to Log K_d of 4 at pH 6, although the surface ratio was signficiantly lower than those used for the model. Despite this, their structures were different, since they identified that the oxide was the primary capture mechanism at the lower pHs and the particle surface concentration of tannin was only half that of the value used in the model. Their work with seawater was also quite different, since the seawater was spiked to concentrations 10^6-10^7 natural levels (e.g. 3‰). Despite all these changes, this work is one of the best for comparison, as they did identify the input conditions sufficiently that it could be simulated using this model. Also recently, McGowan et al. (2022) investigated the sorption of uranium from seawater on a variety of biomass material particles of 2 mm in size e.g. orange skin, diced garlic, potato skin. They observed a very strong sorption of uranium on materials with high phenolic content, particularly with uranyl complexes as reported by Lucks et al. (2012). This data is reported in **Fig. 10**. Much of this data would be considered to be at pH 3-4, as the samples demonstrated fermentation effects of the organics during the sorption process. This effect would also adjust the potential which was not measured at the time.

Fig 9: K_d of U for **v**arious organics from McGowan et al. (2022)]

Zhang et al. (2018), reported data on the adsorption and desorption of uranium (VI) onto humic acids derived from uranium-enriched lignite's in batch experiments. These experiments showed optimum adsorption of uranium (VI) ranged from 5 to 8, although these highly saturated surfaces desorbed at pH values between 1 and 3. The uranium present in the humic acids may not affect the adsorption capacity for U(VI), but the phenolic groups in the humic acids play a significant role in controlling the adsorption capacity, approximately 20 to 30 percent (Ritchie & Perdue, 2003).
Investigation of surface complexation of thorium by humic acid was carried out by Szabo et al. (2006) using chemically immobilized humic acid on silica gel. Thorium (IV) is generally considered as reasonable analogue of uranium(IV). Like with Yu et al. (2022), this means the surface has a second sorption site type, the ratios were not evaluated, the results have to be approximated, for example by combining with the data calculated previously for Degueldre and McGowan (2020).
The Th(IV) sorption isotherm is of a Freundlich type, one can tentatively evaluate K_d of 2 x 10^1 L g^{-1} at pH 4 and 4 x 10^1 L g^{-1} at pH 6 for a total concentration of Th in solution of 1 x 10^{-8} mol L^{-1}. In these conditions (i.e. a nonlinear isotherm), the K_d data at pH 6 for a Langmuir isotherm could be estimated for $K_d = \lim_{C\to 0} K_d = 8 \times 10^1$ L $g^{-1} \approx 1 \times 10^5$ mL g^{-1} (with C the U concentration).
Again, the sorption on particles (inorganic, organic and bioorganic) has been investigated by Li (1981) in seawater conditions. In these conditions at pH 8 and in oxidising conditions, Log K_d was found equal to 4 for U(VI) and 8 for Th(IV), which is generally accepted as an analogous of U(IV), both in carbonated water ($[CO_3]_{Tot}$ =2x10^{-3} M). These values fit reasonably with the data calculated for U(VI) and U(IV), using the values calculated for the dihydroxy-naphthalene developed in this study. It was unusual in that it used similar particle sizes to those used in this model.

5.4 Comparing sorption on polycarboxylics with polyhydroxy-aromatics.

The data gained for the sorption of uranium on polycarboxylic loaded particles were reported in McGowan et al. (2023). These data may be compared with data calculated for polyhydroxy-aromatics (This study)**.**

Clearly the sorption for mono- and multi- dentates surface complexes is stronger for the polyhydroxy-aromatics cases than for polycarboxylics loaded particles. In carbonate free water, at pH 8, the Log K_d are given in Table 12. The sorption coefficients are several orders of magnitude higher in the case of polyhydroxy-aromatics cases compared to the polycarboxylics loaded particles. The E"° for the couple U(VI)/U(IV) is relatively unchanged for the two classes of sorbing group but is more reducing that the E° corresponding to the soluble species (~ -0.15 V).

Table 12: Comparison of the sorption of uranium data on polycarboxylics (see McGowan et al., 2023) and on polyhydroxy-aromatics loaded particles. Conditions: K_d (mL g^{-1}), particles of 0.2 mm size, potential vs NHE, active site density 2-4 nm^{-2} , pH = 8, in carbonated environments ($2x10^{-3}$ M), carboxylic data corrected from site density i.e. 30%.

Surface site	c (-)	U(IV) Log K_d	U(VI) Log K_d	U(VI)/U(IV) E"° (V)
Mono-Carboxylic	1	-01.13	-07.22	-0.54
Bi-Carboxylic	2	-03.81	-09.30	-0.55
Tri-Carboxylic	3	-08.69	-11.18	-0.65
Mono-hydroxy-benzene	2	+03.79	-00.70	-0.59
Di-hydroxy-benzene	2	+08.97	+06.74	-0.69
Di-hydroxy-naphthalene	2	-01.17	-03.57	-0.65

5.5 Factor affecting the hydroxy-aromatics.

As reported by Lund (2021) polyphenols (hydroxy-aromatics) are anti-oxidants. They react as reducing agents with several kind of oxidising reagents, see Farook et al. (2010), Sani et al. (2011), and Vieira da Silva et al. (2013). In the case of uranium, uranyl ions and their complexes yield tetravalent uranium complexes, condensing hydroxyl- groups onto the original phenolic material according to Reaction {12}:

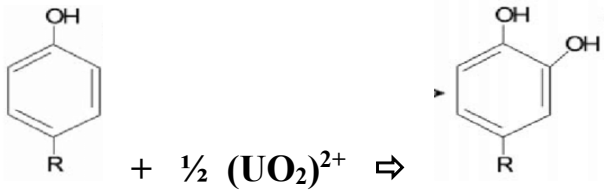

{12}

Uranium is subsequently more strongly complexed onto the surface decorated by polyhydroxy-benzene groups with larger Log K_d values. This is experimentally confirmed by Schmeide et al. (2003) who reported the ability to form chelates for the uranium(VI) indicating a very large increase of its stability constant on coordination to uranium(VI).

6. Conclusions

A model that evaluates for a given pH the sorption coefficient with the redox potential has been developed for prediction of effects of the redox potential on the sorption of uranium onto the three bio-

organic substrates. The model includes surface complexation on multi-dentate surface active sites and complexation with soluble ligands (carbonate) in the aqueous phase and was applied to seawater. The effect of organics were discussed, considering the antagonist properties of carbonates.

Of the three materials, given the theoretical maximum properties described, dihydroxy-naphthalene exhibits the log K_d closest to experimental data from literature, at natural pH and $[CO_3]_{Tot}$ of 8 and 2.2 x 10^{-3} M. This is likely due to the combination of reasonably strong, but more widely spaced bonds of the sites spread over a wider area. Therefore, lower saturations of the other two bonding sites, characterised by a greater *l* value, would also fit this.

Unsurprisingly, increasing $[CO_3]_{Tot}$ decreases the Log K_d. However, as shown experimentally with real organics and in a recent modelling paper (carboxylic group), the carbonate complexes may also co-sorbe under these conditions and polyhydroxy-aromatics would be expected to compensate for any loss in functionality because of their stronger sorbing potential. The calculated Log K_d values were in relative agreement with the scarce experimental values reported in the literature. The sorption analysis so far provides good predictive values for a limited subset of the experimental data, allowing reasonable prediction by modelling of the partition coefficients for a variety of water and biomass sorbents. Such data may rationalise the formation of organic deep sea deposits (U(VI) ⇨ U(IV)) while supporting the oxidation of mono hydroxy- benzene in di-hydroxy-benzene enhancing the sorption of uranium by a factor 10^6. This contribute to sort out a versatile U extraction protocol from seawater. This last objective would require expansion to a wider pool of absorption substrates.

Acknowledgements

This work was performed in the frame of SM PhD thesis which is part of the NGN program partially supported by EPSRC, UK, grant EP/L015390

References

Aihara T., Goto A., Kago T., Kusakabe K. , Morooka S., (1992) Rate of adsorption of uranium from seawater with a calix(6)arene adsorbent . Sep. Sci. Technol., 27: 1655–1667. https://doi.org/10.1080/01496399208029230

Alonso U., Degueldre C., (2003) Modelling americium sorption onto colloids: effect of redox potential, Colloids and Surfaces A, 217: 55-62. https://doi.org/10.1016/S0927-7757(02)00558-7

Bjorkman S., Taylor H. S., (2018) Diethylstilbestrol (DES). In: Encyclopedia of Reproduction (Second Edition). s.l.:s.n

Carbonaro R.F., Atalay Y.B., Di Toro D.M., (2011) Linear Free Energy Relationships for Metal-Ligand Complexation: Bidentate Binding to Negatively-Charged Oxygen Donor Atoms, Geochim Cosmochim Acta. 75: 2499–2511. https://doi.org/10.1016/j.gca.2011.02.027

Degueldre, C., Ulrich, H. J., Silby, H., (1994) Sorption of ^{241}Am onto Montmorillonite, Illite and Hematite Colloids. Radiochimica Acta, 65: 173-179.... https://doi.org/10.1524/ract.1994.65.3.173

Degueldre C., Bilewicz A., Hummel W., Loizeau J.L., (2001) Sorption behaviour of Am on marl groundwater colloids. Journal of Environmental Radioactivity, 55: 241-255. https://doi.org/10.1016/S0265-931X(00)00210-1

Degueldre C., (2016) Uranium as a renewable for nuclear energy, Progress in Nuclear Energy, 94: 17022, https://doi.org/10.1016/j.pnucene.2016.03.031.

Degueldre C. A., Dawson R. J, Najdanovic-Visaka V., (2019) Nuclear fuel cycle, with a liquid ore and fuel: toward renewable energy. Sustainable Energy & Fuels. 3: 1693-1700,. https://doi.org/10.1039/C8SE00610E

Degueldre C., McGowan, S., (2020) Simulating uranium sorption onto inorganic model substrates: effect of redox potential.. J. Environmental Radioactivity, 225: 106408. https://doi.org/10.1016/j.jenvrad.2020.106408

Djogic R., Branica M., (1993) Uranyl mixed-ligand complex formation in artificial seawater. Chemical Speciation & Bioavailability, 5: 101-105. https://doi.org/10.1080/09542299.1993.11083209

Farook A., Radhika T., (2010) Oxidation of benzene over bimetallic Cu–Ce incorporated rice husk silica catalysts, Chemical Engineering Journal, 160: 249-258, https://doi.org/10.1016/j.cej.2010.02.055

Grenthe I., Drozdzynski J., Fujino T., Buck E.C., Albrecht-Schmitt Th. E., Wolf S.,. (2006) Uranium, in: The chemistry of the actinide and transactinide elements. Vol. l.:Springer.

Li Y. H., 1981. Ultimate removal mechanisms of elements from the ocean. Geochim. Cosmochim. Acta, 45: 1659-1664. https://doi.org/10.1016/0016-7037(81)90001-6

Lovley D., Phillips E., Gorby Y., Landa E.R., (1991) Microbial reduction of uranium. Nature 350: 413–416. https://doi.org/10.1038/350413a0.

Lucks C., Rossberg A, Tsushima S, Foerstendorf H, Scheinost AC, Bernhard G., (2012) Aqueous uranium(VI) complexes with acetic and succinic acid: Speciation and Structure Revisited. Inorganic Chemistry, 51, 12288-12300 https://doi.org/10.1021/ic301565p

Lund M.N., (2021) Reactions of plant polyphenols in foods: Impact of molecular structure, Trends in Food Science & Technology, 112; 241-251, https://doi.org/10.1016/j.tifs.2021.03.056.

Martell, A, Smith, R.M., (1989) Critical stability constants, Vol 1-6. Springer-Verlag US (1989).

Mathew B., Jaishankar M., Bij V. G., Beeregowda K. N., (2016) Role of Bioadsorbents in Reducing Toxic Metals. Journal of Toxicology, 13: 4369604. https://doi.org/10.1155/2016/4369604

McGowan, S., Zhang, H., Degueldre, C., (2022) Testing sorption of uranium from seawater on waste biomass: A feasibility study. Fuel, 315: 123224. https://doi.org/10.1016/j.fuel.2022.123224

McGowan S., Degueldre C., Aiouache F., (2023) Modelling the reaction of uranium with carboxylic groups on surfaces through mono- and multi- dentate surface complexes on the basis of pH and redox potential, Colloid & Surface C., 1: 100002. https://doi.org/10.1016/j.colsuc.2023.100002

McKinley, I., Scholits, A., (1993) A comparison of radionuclide sorption databases used in recent performance assessments. Journal of Contaminant Hydrology, 13: 347-363. https://doi.org/10.1016/S0265-931X(00)00210-1

Millero, F., (2013) Chemical oceanography..:CRC press..

NEA, (2004) Chemical thermodynamics of uranium, Data bank Radioactive waste management, s.l.: OECD/NEA.

NEA and IAEA, (2016) Uranium 2016 - resource, production and demand. OECD publishing p. 548..

Pontoni L., La Vecchia, C., Boguta, P., Sirakov M., D'Aniello E., Fabbricino M., Locascio A., (2022) Natural organic matter controls metal speciation and toxicity for marine organisms: a review. Environ Chem Lett , 20: 797–812. doi.org/10.1007/s10311-021-01310-y

Rérolle V. ,Floquet C.F.A., Mowlem M.C. M.C., Connelly D.P., Achterberg E.P., Bellerby R.R.G.J.., (2012) Seawater-pH measurements for ocean-acidification observations. TrAC. Trends in Analytical Chemistry, 40: 146-157. https://doi.org/10.1016/j.trac.2012.07.016 .

Ritchie J. D., Perdue E. M., (2003) Proton-binding study of standard and reference fulvic acids, humic acids, and natural. Geochimica et Cosmochimica Acta, 67: 85-96. https://doi.org/10.1016/S0016-7037(02)01044-X

Sakagushi T., Nakajima A., (1987) Recovery of uranium from seawater by immobilized tannin. Separat. Sci. Technol., 22: 1609-1623. https://doi.org/10.1080/01496398708058421

751 Saleem M., Kim H., Ali M. S., Lee Y., (2005) An update on bioactive plant lignans. Natural Product Reports,
752 22: 696-716. https://doi.org/10.1039/B514045P

753 Sani S., Mohd Muhid M.N., Hamda, H. (2011) Design, synthesis and activity study of tyrosinase encapsulated
754 silica aerogel (TESA) biosensor for phenol removal in aqueous solution. J Sol-Gel Sci Technol, 59: 7–18.
755 https://doi.org/10.1007/s10971-011-2454-3

756 Sharp, J, Byrne, R., Liu X., Feely R.A., Cuyler E.E., Wanninkhof R., Alin S., (2017) Spectrophotometric
757 Determination of Carbonate Ion Concentrations: Elimination of Instrument-Dependent Offsets and Calculation
758 of In Situ Saturation States. Environ. Sci. Technol., 51: 9127–9136. https://doi.org/10.1021/acs.est.7b02266

759 Schenk H. J., Astheimer L., Witte E. G., Schwochau K., (1982) Development of Sorbers for the Recovery of
760 Uranium from Seawater. 1. Assessment of Key Parameters and Screening Studies of Sorber Materials.
761 Separation Science and Technology, 17: 1293-1308. https://doi.org/10.1080/01496398208056103

762 Schmeide K., Sachs S., Bubner M., Reich T., Heise K.H., Bernhard G., (2003) Interaction of uranium(VI) with
763 various modified and unmodified natural and synthetic humic substances studied by EXAFS and FTIR
764 spectroscopy. Inorganica Chimica Acta. 351: 133-140. https://doi.org/10.1016/S0020-1693(03)00184-1

765 Sekiguchi K., Saito K., Konishi S., Furusaki S., Sugo T., Nobukawa H., (1994) Effect of seawater temperature
766 on uranium recovery from seawater using amidoxime adsorbents . Ind. Eng. Chem. Res., 33: 662 - 666.
767 https://doi.org/10.1021/ie00027a025

768 Senko J.M., Istok J.D., Suflita J.M., Krumholzan L. R., (2002) In-Situ Evidence for Uranium Immobilization
769 and Remobilization, Environ. Sci. Technol., 36: 1491–1496. https://doi.org/10.1021/es011240x.

770 Szabó Gy., Guczi J., Reiller P., Geckeis H., Bulman R. A. (20069 Investigation of complexation of thorium by
771 humic acid using chemically immobilized humic acid on silica gel. Radiochimica Acta, 94: 553-557.
772 https://doi.org/10.1524/ract.2006.94.9-11.553

773 Ververidis F. F., Trantas E., Douglas C., Vollmer G., Kretzschmar G., Panopoulos N., (2007) Biotechnology of
774 flavonoids and other phenylpropanoid-derived natural products. Part I: Chemical diversity, impacts on plant
775 biology and human health. Biotechnology Journal, 2: 1214–1234. https://doi.org/10.1002/biot.200700084

776 Vieira da Silva L.V., Tavares A.P, Kameda E.. Macedo E.A., Coelho M. A., Amaral, Pr.F., (2013) Factors
777 affecting water colour removal by tyrosinase. International Journal of Environmental Studies. 70: 316-326.
778 https://doi.org/10.1080/00207233.2013.783267

779 Yamashita H., Ozawa Y., Nakajima F., Murata T., (1980) The collection of uranium from seawater with
780 hydrous metal oxide. III. The effects of diverse ions in seawater on uranium adsorption by hydrous titanium(IV)
781 oxide. Bull. Chem. Soc. Jpn., 53: 1331 – 1334. https://doi.org/10.1246/bcsj.53.1331

782 Yu J., Yu C., Zhu W.,.He G., Wei Y., Zhou J., (2022) Hydrous titanium oxide and bayberry tannin co-
783 immobilized nano collagen fibrils for uranium extraction from seawater and recovery from nuclear wastewater.
784 Chemosphere, 286: 131626. https://doi.org/10.1016/j.chemosphere.2021.131626

785 Zhang A., Uchiyama G., Asakura, T., (2005) pH Effect on the uranium adsorption from seawater by a
786 macroporous fibrous polymeric material containing amidoxime chelating functional group. React. Funct.
787 Polym., 63: 143 – 153. https://doi.org/10.1016/j.reactfunctpolym.2005.02.015 .

788 Zhang Y, Li Y, Ning Y, Liu D, Tang P, Yang Z, Lu Y, Wang X., (2018) Adsorption and desorption of
789 uranium(VI) onto humic acids derived from uranium-enriched lignites. Water Sci Technol. 77: 920-930.
790 https://doi.org/10.2166/wst.2017.608.

791

792